PAPER

The KATRIN pre-spectrometer at reduced filter energy

New Journal of Physics
The open-access journal for physics

The KATRIN pre-spectrometer at reduced filter energy

M Prall[1,8], P Renschler[2], F Glück[2,3], A Beglarian[2], H Bichsel[4], L Bornschein[2], Z Chaoui[5], G Drexlin[2], F Fränkle[2,7], S Görhardt[2], S Mertens[2], M Steidl[2], Th Thümmler[2], S Wüstling[2], C Weinheimer[1] and S Zadorozhny[6]

[1] Institut für Kernphysik, Universität Münster, Wilhelm-Klemm-Straße 9, 48149 Münster, Germany
[2] KCETA, Karlsruhe Institute of Technology, PO Box 3640, 76021 Karlsruhe, Germany
[3] KFKI, RMKI, H-1525 Budapest, PO Box 49, Hungary
[4] CENPA, University of Washington, PO Box 354290, Seattle, WA 98195-4290, USA
[5] Laboratory of Optoelectronics and Devices, Faculty of Science, University of Setif, Algeria
[6] Institute for Nuclear Research of Russian Academy of Sciences, Moscow, Russia
[7] Department of Physics, University of North Carolina, Chapel Hill, NC, USA
E-mail: matthias.prall@uni-muenster.de

New Journal of Physics **14** (2012) 073054 (22pp)
Received 5 March 2012
Published 27 July 2012
Online at http://www.njp.org/
doi:10.1088/1367-2630/14/7/073054

Abstract. The Karlsruhe Tritium Neutrino (KATRIN) experiment will determine the mass of the electron neutrino with a sensitivity of 0.2 eV (90% CL) via a measurement of the β-spectrum of gaseous tritium near its endpoint of $E_0 = 18.57$ keV. An ultra-low background of about $b = 10$ mHz is among the requirements on reaching this sensitivity. In the KATRIN main beam line, two spectrometers of MAC-E filter type are used in tandem configuration. This setup, however, produces a Penning trap, which could lead to increased background. We have performed test measurements showing that the filter energy of the pre-spectrometer can be reduced by several keV in order to diminish this

[8] Author to whom any correspondence should be addressed.

trap. These measurements were analyzed with the help of a complex computer simulation, modeling multiple electron reflections from both the detector and the photoelectric electron source used in our test setup.

Contents

1. Introduction

The observation of flavor oscillations of atmospheric, solar, reactor and accelerator neutrinos has provided convincing evidence for lepton mixing and non-zero neutrino masses. However, neutrino oscillation studies only allow us to access the mass splittings of various neutrino mass eigenstates, but yield no information on the absolute neutrino mass scale. The latter is of fundamental importance for both cosmology and particle physics. In cosmology, neutrinos as hot dark matter could play a role in the evolution of galaxies. In particle physics, the determination of the mass scale would help discriminate among different neutrino mass models, such as scenarios with hierarchical or quasi-degenerate masses.

There are various methods and techniques for accessing the absolute neutrino mass scale. Galaxy redshift surveys and observations of the cosmic mircowave background provide information on the large-scale structure of the universe, from which a stringent upper limit of about 0.5 eV for the sum of all neutrinos has been derived [1]. In addition, neutrinoless double β-decay experiments at present reach neutrino mass sensitivities of less than 1 eV, and could attain 100 meV or even better sensitivities in future [2, 3]. However, theoretical interpretations of these observations and experiments are rather model dependent.

Measurement of the electron energy spectrum close to the endpoint of nuclear β-decays (tritium, ^{187}Re) is the only direct and model independent way of determining the absolute neutrino mass scale [4], relying only on the relativistic energy–momentum relation and energy conservation. The Karlsruhe Tritium Neutrino (KATRIN) experiment is a next-generation, tritium β-decay experiment. It is currently under construction at the Karlsruhe Institute of Technology and is designed to measure the 'effective electron neutrino mass' with a sensitivity of 200 meV. Among other parameters, a low background level of 10 mHz is required for obtaining this sensitivity.

A non-zero neutrino mass distorts the electron energy spectrum shape of tritium β-decay, and this spectrum will be analyzed by KATRIN close to the endpoint by two electrostatic retarding spectrometers of the MAC-E filter type: the pre-spectrometer (PS) and the much larger main spectrometer (MS). The PS offers the option to act as a pre-filter, reflecting all β-electrons up to 300 eV below the endpoint, while transmitting the interesting part of the spectrum without modification. All electrons transmitted through this first stage are guided to the MS for precise energy analysis. The exceedingly large dimensions of the MS allow us to operate it as an extremely precise high-energy filter with an energy resolution of $\Delta E = 0.93$ eV, kept on a stable high voltage in the ppm range.

The operation of two electrostatic retarding spectrometers in a beamline poses several challenges. The two spectrometers are set on a high negative potential next to each other, with ground potential and high magnetic field between them. This configuration will create a deep Penning trap for electrons. Signal electrons that experience no energy loss on their passage in the spectrometers are not affected by this trap. However, electrons that are generated in between the spectrometers with a lower kinetic energy than the PS filter energy are trapped. Ionizational collisions of these trapped electrons with residual gas molecules will significantly increase the background, thus reducing the neutrino mass sensitivity of the experiment.

A possible countermeasure for alleviating this background[9] is to avoid the creation of the Penning trap by reducing the filter voltage $|U_{\mathrm{PS}}|$ of the PS down to low values, even zero in the most extreme case. The goal of this paper is to test the feasibility of this option by studying the transmission properties of electrons with large surplus energies both experimentally and with extensive Monte Carlo (MC) simulations. These investigations revealed that the KATRIN PS has excellent transmission properties even when operating it at reduced filter energy.

This paper is organized as follows. In section 2 we present the KATRIN setup, in section 3 the operating principle of the MAC-E filter is reviewed; section 4 presents our experimental setup; our measurements and their analysis using custom simulation tools are presented in sections 5–7. Section 8 discusses the background and adiabaticity at reduced PS filter energy in detail. Finally, our findings are summarized in section 9.

2. The Karlsruhe Tritium Neutrino experiment

The KATRIN experiment [5] will determine the mass of the electron antineutrino[10] $m_{\nu_e}^{(\mathrm{eff})} = \sqrt{\sum m_i^2 |U_{\mathrm{ei}}|^2}$ via a high-precision measurement of the β-decay kinematics at the endpoint $E_0 = 18.57$ keV of the β-spectrum of tritium with a sensitivity of 0.2 eV (90% CL). The latest upper limits obtained with this model-independent method and the isotope tritium as a β-emitter are from the experiments at Mainz: $m_{\nu_e}^{(\mathrm{eff})} < 2.3$ eV (95% CL) [6] and at Troitsk: $m_{\nu_e}^{(\mathrm{eff})} < 2.05$ eV (95% CL) [7]. Figure 1 shows a schematic overview over the 70 m long KATRIN setup: T_2 gas with an activity of 10^{11} Bq is recirculated in the so-called windowless gaseous tritium source (WGTS). β-decay electrons are guided by a magnetic field toward the spectrometers. Both the pre- and the MS are of the MAC-E filter type [8].

[9] Another countermeasure is to remove stored electrons in the Penning trap mechanically by a wire scanner or a fixed pin [9].

[10] KATRIN will not be able to resolve the different neutrino mass eigenstates m_i, but will determine a weighted average $m^{(\mathrm{eff})}$ of the neutrino mass states m_i according to their mixing U_{ei} with the electron neutrino.

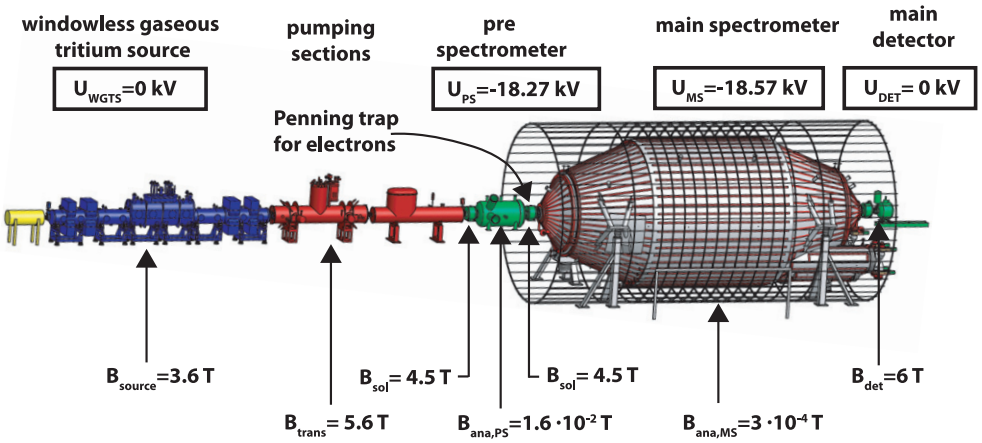

Figure 1. Overview of the KATRIN experiment with the potentials and magnetic field strengths given in the KATRIN design report [5]. With these values, the setup contains a Penning trap for electrons between the pre- and the MS at $B_{\mathrm{sol}} = 4.5\,\mathrm{T}$. A change of the PS potential from $U_{\mathrm{PS}} = -18.27\,\mathrm{kV}$ by several kV toward smaller absolute values will diminish this trap.

Electrons are guided through these spectrometers along the magnetic field lines and are decelerated by an electric filter potential U_{f} in each of the spectrometers. U_{f} is the high voltage with negative polarity applied to the spectrometer, or more exactly, to its inner electrode system [5]. In KATRIN, we use the independent filter potentials $U_{\mathrm{f}} = U_{\mathrm{PS}}$ for the PS and $U_{\mathrm{f}} = U_{\mathrm{MS}}$ for the MS. Only those electrons with an energy E larger than the filter energy qU_{f} (see section 3) are transmitted through a spectrometer and are reaccelerated to their original energy. Here $q = -e$ is the negative electron charge, and the filter energy qU_{f} is the maximum potential energy of an electron in the spectrometers. The PS with an energy resolution of $\Delta E_{\mathrm{PS}} \approx 100\,\mathrm{eV}$ is the first filter for the β-decay electrons. It reduces the flux of β-decay electrons into the MS, lowering the rate of background electrons created in collisions with residual gas molecules [5]. Having an energy resolution of $\Delta E_{\mathrm{MS}} = 0.93\,\mathrm{eV}$, the MS scans the last 30 eV of the T_2 β-spectrum which contain information on the neutrino mass. Finally, the electrons transmitted by the MS are counted by a 148-pixel PIN diode with an energy resolution of $\Delta E_{\mathrm{det}} \approx 1\,\mathrm{keV}$.

The motivation for our investigations is the following: inside the MS, the β-decay electrons can start multi-step processes leading to free electrons. These can be accelerated toward the detector and to energies around 18 keV by the MS potential. The energy resolution of KATRIN's detector is about $\Delta E_{\mathrm{det}} \approx 1\,\mathrm{keV}$. Therefore, these electrons cannot be distinguished from signal electrons produced by the tritium β-decay. Thus, the background can rise above KATRIN requirements of $b = 10\,\mathrm{mHz}$ [5]. Therefore, the flux of β-decay electrons into the MS should be kept low. The flux of β-electrons can be minimized by keeping the filter potentials of MS and PS relatively close (e.g. $U_{\mathrm{PS}} = -18.27\,\mathrm{kV}$ and $U_{\mathrm{MS}} \approx -18.57\,\mathrm{kV}$). However, using the B-fields ($B_{\mathrm{sol}} = 4.5\,\mathrm{T}$, figure 1) mentioned in the KATRIN design report [5] the region between the two spectrometers is a Penning trap for electrons. By multi-step processes this trap can lead to increased background as well [9]. A reduction of the PS potential from $U_{\mathrm{PS}} = -18.27\,\mathrm{kV}$ by several kV toward smaller absolute values will diminish this trap. The optimum value of U_{PS} that minimizes the background has to be determined experimentally. If qU_{PS} is reduced by several

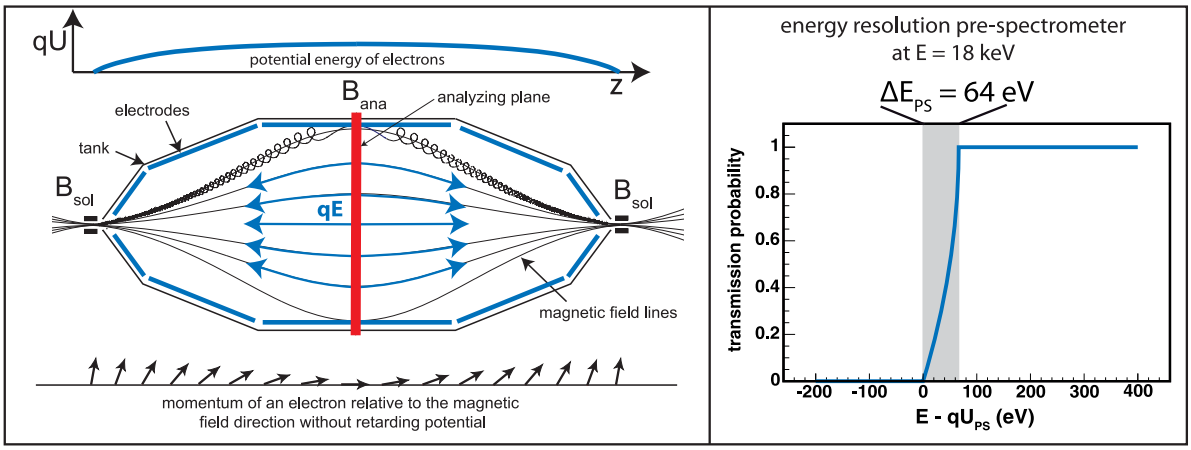

Figure 2. Left: working principle of a MAC-E filter. Right: ideal transmission function of the PS for an isotropic source of monoenergetic electrons with $E_0 = 18.57\,\mathrm{keV}$, $B_{\mathrm{ana,PS}} = 0.016\,\mathrm{T}$ and $B_{\mathrm{sol}} = 4.5\,\mathrm{T}$. The transmission probability of the PS (of an MAC-E filter) starts becoming non-zero as soon as the energy E of the incoming electron is larger than the filter energy qU_{PS}. Both the tank and the electrodes of the KATRIN PS and the MS are on negative high voltage. Detailed explanations can be found in the main text.

keV however, the β-electrons with energies close to $E_0 = 18.57\,\mathrm{keV}$ will retain a surplus energy $E_{\mathrm{sur}} = E_0 - qU_{\mathrm{PS}}$ of the order of several keV inside the PS. Thus, electrons have higher speed and may no longer be guided by the magnetic field. This behavior, leading to transmission losses, was already observed in the MAC-E filter of the Mainz Neutrino Mass Experiment [10, 11]. For KATRIN, 100% transmission above the PS filter energy qU_{PS} is required. We present two main results in this paper:

1. The requirement for 100% transmission at reduced PS filter energy qU_{PS} is fulfilled. If it should turn out that the Penning trap between the two spectrometers cannot be suppressed by other means [9], the PS filter energy can be reduced by many keV in order to overcome this problem.
2. The KATRIN collaboration is able to model the electron transport and the electron backscattering at the detector with high precision in agreement with experimental data. This allows detailed investigations of the experimental setup.

3. The MAC-E filter technique

In this section, we explain the principle of a MAC-E filter [8] under standard conditions, i.e. when the filter energy qU_{f} is close to (a few tens of eV) the energy E of the incoming electrons.

The principle of a MAC-E filter is illustrated in figure 2: two identical solenoids provide a guiding magnetic field. Ignoring drift motions which appear as higher order corrections [12], the β-electrons enter the MAC-E filter and follow the guiding magnetic field lines along helix-like trajectories resulting from the cyclotron motion. This statement holds true if the relative

changes of the electric and magnetic field strength within a cyclotron length l_{cyc} are small [12]:

$$\begin{aligned} &\tfrac{|\Delta\vec{E}|}{|\vec{E}|} \ll 1 \quad \text{and} \quad \tfrac{|\Delta\vec{B}|}{|\vec{B}|} \ll 1, \\ &\text{within one cyclotron length} \\ &l_{\mathrm{cyc}}\colon \quad l_{\mathrm{cyc}} = 2\pi \tfrac{v_\parallel}{\omega_{\mathrm{cyc}}} = 2\pi \tfrac{\gamma m_{\mathrm{e}}}{|q|B} v_\parallel . \end{aligned} \tag{1}$$

Here, $v_\parallel$ is the electron velocity parallel to the guiding magnetic field line, ω_{cyc} the cyclotron frequency, m_{e} the electron mass, $q = -e$ the negative electron charge and γ the relativistic factor.

If equation (1) holds, there is a conserved adiabatic invariant $\gamma\mu$, where μ denotes the orbital magnetic moment of the electron (see section 12.5 of [13])

$$\mu = \frac{\gamma + 1}{2\gamma} \cdot \frac{E_\perp}{B} = \frac{p_\perp^2}{2m_{\mathrm{e}}\gamma B}. \tag{2}$$

$E_\perp = E_{\mathrm{kin}} \cdot \sin^2(\theta)$ is the fraction of the kinetic energy E_{kin} that can be attributed to the motion around the guiding B-field line. θ is the polar angle between the guiding B-field line and the electron momentum vector. In the following, we will use the symbol φ for the corresponding azimuthal angle. $E_\parallel = E_{\mathrm{kin}} \cdot \cos^2(\theta)$ is the fraction of the kinetic energy connected to the forward motion of the electron. Only $E_\parallel$ is analyzed by the MAC-E filter. $p_\perp$ denotes the fraction of the electron momentum perpendicular to the guiding B-field line.

For KATRIN, the maximum electron energy is $E_0 = 18.57\,\mathrm{keV}$; thus one has $\gamma \leqslant 1.04$. Therefore, μ is a good approximation for the conserved quantity, especially when electrons are slowed down by the electric field in the MAC-E filter:

$$\mu \approx \frac{E_\perp}{B} = \frac{E_{\mathrm{kin}} \cdot \sin^2\theta}{B} \approx \text{const.} \tag{3}$$

From equation (3) it is clear that the polar angle θ and $E_\perp$ are completely determined by the B-field and the kinetic energy of the electron. When B decreases toward the analyzing plane of the MAC-E filter, $E_\perp$ is minimized, providing a good energy resolution of the MAC-E filter. Electrons are guaranteed to be transmitted along the guiding B-field line if their initial energy is large enough to overcome the spectrometer potential. The transmission probability $T(E, qU_{\mathrm{f}})$ of a MAC-E filter is derived from equation (3) by integrating over all electrons that fulfill $0 < E_\parallel = (E - qU_{\mathrm{f}}) - E_\perp$ in the central plane of the MAC-E filter. These electrons start at the ground potential. Isotropically emitted electrons with a starting energy E and a θ from 0° to 90° have to be considered. Equation (2) is used to transform between $E_\perp$ at the origin of the electrons with B_{s} and the analyzing plane, with the minimum B-field strength B_{ana}:

$$T(E, qU_{\mathrm{f}}) = 1 - \sqrt{1 - \frac{E - qU_{\mathrm{f}}}{E} \cdot \frac{B_{\mathrm{s}}}{B_{\mathrm{ana}}}} \quad \text{for} \quad qU_{\mathrm{f}} \leqslant E \leqslant qU_{\mathrm{f}} \cdot \frac{B_{\mathrm{s}}}{B_{\mathrm{s}} - B_{\mathrm{ana}}}. \tag{4}$$

Thus, the transmission probability $T(E, qU_{\mathrm{f}})$ only depends on the magnetic field strengths, on the energy E of the incoming electron and on qU_{f}, the filter energy. Below the interval specified in equation (4), the transmission probability is zero; above this interval it is unity (figure 2). The transmission function describes an energy high-pass filter; only electrons with an energy E above the filter potential qU_{f} are transmitted. The energy resolution of the MAC-E filter ΔE_{f} is equal to the maximum $E_\perp$ of an electron in its analyzing plane. $E_\perp$ in the analyzing

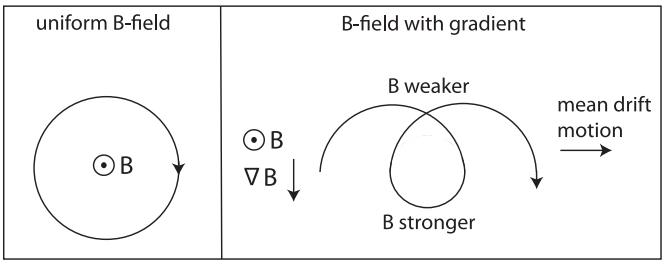

Figure 3. Pictorial explanation of the Grad B × B-drift. Left: the orbit of a charged particle in a uniform B-field. Right: the orbit of a charged particle in a non-uniform B-field.

plane is maximal if the polar angle θ is equal to 90° in the entry-side magnet. The conservation of μ allows us to compute the resolution ΔE_{f}:

$$\text{const} \approx \mu = \frac{E_{\perp}}{B} \Longrightarrow \Delta E_{\mathrm{f}} = E \cdot \frac{B_{\mathrm{ana}}}{B_{\mathrm{s}}}. \tag{5}$$

Considering electrons starting in the entry-side solenoid of the PS, one has to insert $B_{\mathrm{s}} = B_{\mathrm{sol}} = 4.5\,\mathrm{T}$ and $B_{\mathrm{ana,PS}} = 0.016\,\mathrm{T}$. The formula gives an energy resolution $\Delta E_{\mathrm{PS}} = 64\,\mathrm{eV}$ if the PS is used with $E = 18\,\mathrm{keV}$ electrons (cf figure 2(right)). For a MAC-E filter and in the adiabatic approximation [12], the Lorentz force

$$\vec{F} = q(\vec{E} + \vec{v} \times \vec{B}) \tag{6}$$

results not only in a helix-like motion around the guiding magnetic field line but also in an azimuthal magnetron drift around the spectrometer symmetry axis [8].

Electrons that pass the MAC-E filter on its symmetry axis gyrate around the central magnetic field line in a helical cyclotron motion. Since the magnetic field is axially symmetric and the cyclotron radius is changing slowly, the electrons are in a quasi-constant magnetic field. For off-axis electrons, however, the magnetic field is asymmetric during a cyclotron motion. The radius of curvature of the electron trajectory is smaller in a stronger B-field. Therefore, the gradient $\vec{\nabla} B$ results in an azimuthal $\vec{B} \times \vec{\nabla} B$ drift of the guiding center along a circle with constant magnetic field (figure 3):

$$\vec{v}_{\perp} = \frac{1}{qB}\left(E_{\perp} + 2 \cdot E_{\parallel}\right) \cdot \frac{\vec{B} \times \vec{\nabla} B}{B^2}. \tag{7}$$

The lower the qU_{PS} in our investigations, the larger the $E_{\perp}$ and $E_{\parallel}$ and azimuthal drift (7). Section 4 will show that our PS data can be understood only if the azimuthal drift (7) is taken into account.

4. The pre-spectrometer test setup

This section describes the experimental setup used for measuring the PS transmission with $E = 18\,\mathrm{keV}$ electrons and a PS filter energy qU_{PS} down to 1 keV, so that the electrons retain a surplus energy $E_{\mathrm{sur}} = E - qU_{\mathrm{PS}}$ of up to 17 keV in the PS.

The B-field of the PS test setup (figure 4) is generated by two solenoids (B). The inner electrode system of the PS tank (G) consists of four parts: the ground electrodes (C) define the

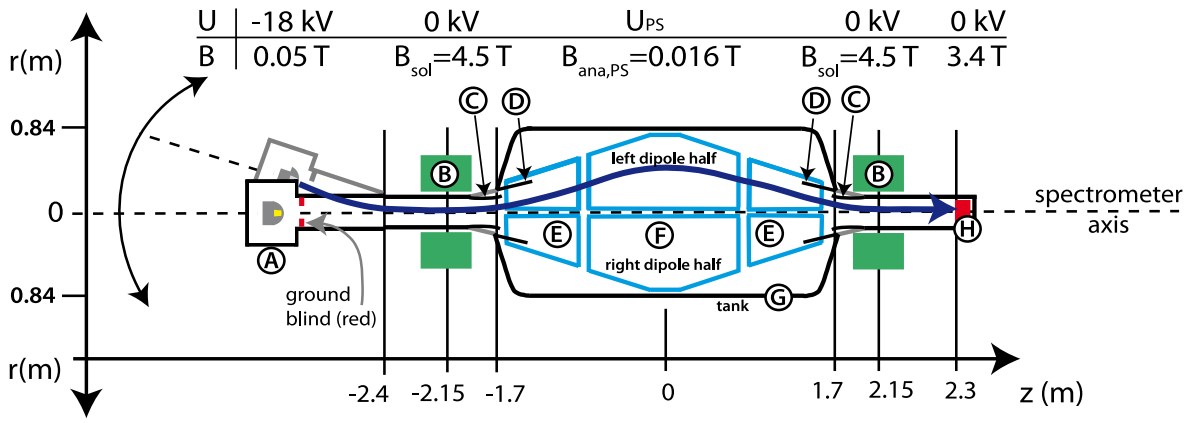

Figure 4. The PS test setup: (A) a photoelectric electron source (E-GUN), (B) a solenoid, (C) a ground electrode, (D) a shielding electrode, (E) a full metal cone electrode, (F) a wire electrode, (G) a spectrometer vessel and (H) a 64-pixel silicon PIN diode. There is a longitudinal gap splitting electrodes (E) and (F) into a left half and a right half. For our measurements, the left and right dipole halves were electrically connected and therefore supplied with identical voltages. The dark blue arrow illustrates an electron trajectory.

potential at the entry and the exit of the PS, the shielding electrodes (D) were introduced to avoid a Penning trap leading to the background [14], electrodes (E) are conical metal shields and the central part (F) is a wire electrode. The tank (G) and the shielding electrodes (D) are electrically connected. Both the tank and the electrodes are on negative high voltage. There is a longitudinal gap splitting electrodes (E) and (F) into a left and a right half. For our measurements, the left and right dipole halves were electrically connected and therefore supplied with identical voltages. Previous measurements [14] with this setup and a pressure of 10^{-10} mbar inside the PS resulted in an average background rate of 17 ± 0.4 mHz in the energy window from 15 to 21 keV over the whole detector. For these, the tank (G) and the shielding electrode (D) were kept at $U_{\text{tank}} = -18$ kV, and the inner electrodes (E) and (F) were put on $U_{\text{electrode}} = -18.5$ kV. As this configuration does not produce any background related to particles stored in Penning traps, the same potential difference $U_{\text{electrode}} - U_{\text{tank}} = -0.5$ kV between the tank (G) and the electrode system (E, F) was used in our measurements. The potential inside the PS tank is a mixture of the electrode and tank potentials; so one has $U_{\text{PS}} = a \cdot U_{\text{tank}} + b \cdot U_{\text{electrode}}$. However, the constants are $a = 0$ and $b = 1$ in good approximation. U_{PS} and $U_{\text{electrode}}$ never differ by more than a few tens of V. This effect depends on the electron trajectory in the PS and is accounted for in our simulations (section 7). For these, we have computed the actual electric field inside the PS using the methods described in [15, 16]. In the following we do not distinguish between qU_{PS} and $qU_{\text{electrode}}$ in the text, as their difference is negligible at keV surplus energies. In each of our measurement series, the tank voltage U_{tank} was varied from -0.5 kV to about -17.5 kV, so that the PS filter energy $qU_{\text{PS}} \approx qU_{\text{electrode}}$ varied from about 1 keV to about 18 keV.

A photoelectric electron source (E-GUN) (figure 5) mounted at the entry of the PS test setup (figure 4) was used to generate electrons with an energy of $E = 18$ keV for the measurements: a deuterium lamp (f) generates UV light with wavelengths in the range of $185\,\text{nm} < \lambda < 400\,\text{nm}$ ($6.7\,\text{eV} > h\nu > 3.1\,\text{eV}$). The light shines through a sapphire window

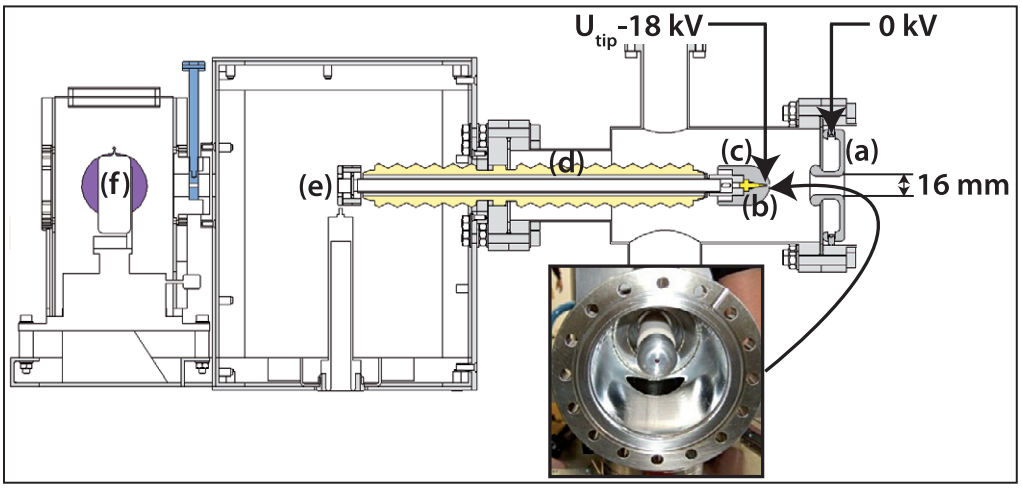

Figure 5. The photoelectric electron source (E-GUN). (a) The ground blind (diameter of the bore = 16 mm), (b) a gold-plated quartz tip at $U_{\text{tip}} = -18$ kV (yellow), (c) the metal housing (grey), (d) an insulator, (e) a sapphire window and (f) a deuterium UV lamp. The inset shows the metal housing, which includes the gold-plated quartz tip. Here, the ground blind was removed.

(e) and a hollow ceramic insulator (d). The UV photons finally produce free electrons via the photoelectric effect in a thin gold layer ($\approx 35\,\mu\text{g cm}^{-2}$) on a gold-plated quartz tip (b) sitting in a metal housing (c). The quartz tip is transparent to light of wavelength $150\,\text{nm} < \lambda < 4000\,\text{nm}$, thus not cutting into the UV spectrum of the deuterium lamp. The work function of gold is 4.83 ± 0.02 eV [17]. Therefore, only those electrons with excess energies of up to $E_{\text{max}} = 6.7\text{–}4.83\,\text{eV} = 1.87\,\text{eV}$ can be released. The gold plated tip is supplied with a voltage of $U_{\text{tip}} = -18$ kV. The photoelectrons are finally accelerated to an energy of $qU_{\text{tip}} = 18$ keV in the forward direction by a blind (a) on the ground potential.

The electron source is mounted on a manipulator, which allowed us to move it on a sphere up to $\alpha \pm 19^\circ$ into the horizontal and vertical directions (cf figure 4). This corresponds to a motion for the gold-plated tip on a radius of 1.06 m around the point with the PS coordinates $z = -2.4$ m and $r = 0$ m, 0.25 m behind the center of the source magnet (cf figure 4). The intensity stability of the electron source was measured to better than 0.2% per hour. Figure 5 shows the cross-section of the E-GUN. The reader should keep in mind that the electric field near the gold-plated tip (b) is strong and there is a ground blind (a) mounted in front of the tip. Together with the electric and magnetic fields inside the E-GUN and the detector, these two components have an important role in our data analysis (section 7).

The PS detector is a quadratically segmented silicon PIN diode with 64 pixels of equal size and properties. It has an overall sensitive area of $16\,\text{cm}^2$ [18]. It is a predecessor of the final KATRIN detector and was manufactured with the same processing techniques. For simulations of the detector response, the energy resolution ΔE_{FWHM} and the dead layer thickness λ have to be known. The detector system exhibited a measured average $\Delta E_{\text{FWHM}} \approx 3.5$ keV. The thickness of the dead layer was determined to be $\lambda = 119 \pm 3$ nm and $\lambda = 109 \pm 3$ nm by using two independent experimental techniques [19]. The detector is located at $z = 2.3$ m (15 cm behind the central plane of the detector magnet) at $B = 3.4$ T and at ground potential (figure 4).

Table 1. Summary of measurements.

B_{sol} (T)	r_{cen} (cm)	Scans	Measurement time (s)	Events at $qU_{electrode} = 17.5\,keV$
	0	5	478	1.9×10^6
4.5	41.4	3	287	1.0×10^6
	52.3	4	380	1.3×10^6
	0	3	287	1.0×10^6
2.3	41.4	4	414	1.0×10^6
	52.3	2	192	0.4×10^6

If the detector is centered on the PS axis, its area corresponds to 28.5% of KATRIN's magnetic flux tube. In our measurements, the detector was adjusted laterally so that only a single pixel was hit and the data analysis was made with this single pixel. The energy calibration of the pixel was used to select events in the region of interest from 15 keV to 21 keV.

For our measurements, the inner electrodes (E) and (F) (cf figure 4) were put on a voltage of $U_{electrode} - U_{tank} = -500 \pm 0.1$ V with respect to the PS tank using a voltage supply (Canberra 3101/2) mounted inside a rack on tank potential. The tank voltage itself (U_{tank} between -0.5 kV and -17.5 kV) was supplied by another voltage source (FUG HCN 140M-35000). The gold-plated tip of the E-GUN was supplied with a constant voltage of $U_{tip} = -18$ kV by a high-voltage supply (FUG HCN 35-35000). The accuracy of the voltage difference determination between the tank and the gold-plated tip was better than 10 V.

5. Measurements

We carried out six measurement series with $E = 18$ keV electrons (table 1). The PS solenoids were set to the KATRIN design value of $B_{sol} = 4.5$ T (figures 1 and 4) and half this value $B_{sol} = 2.3$ T. As the cyclotron length grows with $1/B$ (equation (1)), deviations from the ideal transmission properties described in section 3 are more probable for the decreased B-field $B_{sol} = 2.3$ T. The electrons pass the PS on a radius $r(z)$, which encloses a constant magnetic flux ϕ_{enc} (in a homogeneous B-field, one has $\phi_{enc} \approx \pi \cdot r^2(z) \cdot B(z)$). For each B-field, the PS transmission was measured for three different angular positions ($\alpha \in \{0°, 15°, 19°\}$) of the E-GUN (cf figure 4). With the given angles α, electrons pass the central plane of the PS at the radii $r_{cen} \in \{0\,cm, 41.4\,cm, 52.3\,cm\}$. At the KATRIN design value $B_{sol} = 4.5$ T, the corresponding fraction $f = \phi_{enc}/\phi_{KAT}$ of the enclosed KATRIN flux tube $\phi_{KAT} = 191\,T \cdot cm^2$ is $f \in \{0\%, 45\%, 72\%\}$.

In each measurement series, the PS filter energy qU_{PS} was stepped repeatedly from 1 keV toward 18 keV and back to 1 keV, using identical time intervals. Combining the counts from the ramp up and the ramp down eliminates a possible linear drift in the emission rate of the E-GUN. Each detector run at a constant potential lasted for about $R = 48$ s. The procedure was repeated up to five times (see 'Scans' in table 1), resulting in an overall measurement time of e.g. $478\,s \approx scans \cdot 2 \cdot R$ for a measurement with $B_{sol} = 4.5$ T and $r_{cen} = 0$ cm. From runs with identical voltages, r_{cen} and B-field settings, electron events were summed and divided by the overall measurement time to obtain the average electron rate. The detector was adjusted laterally before the start of the measurements so that only a single detector pixel was hit.

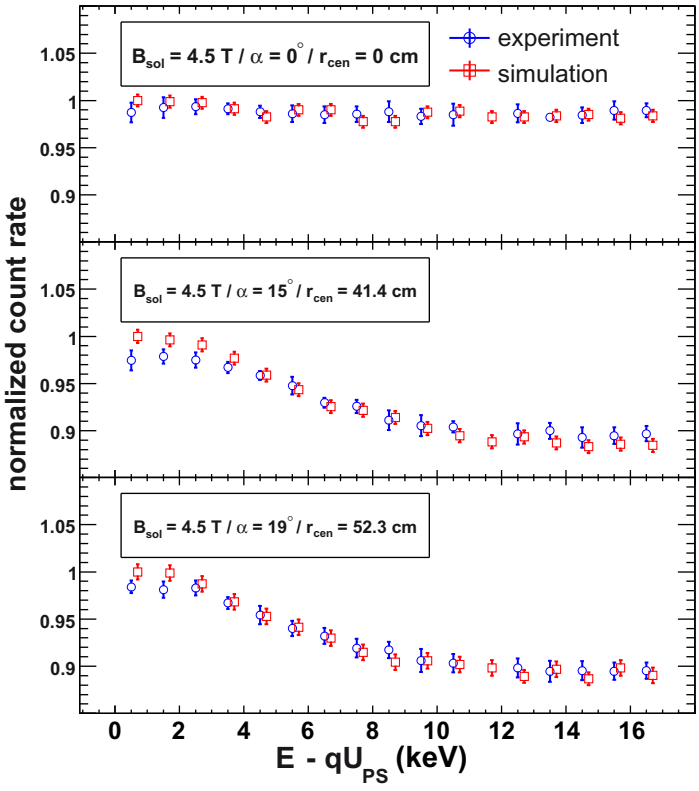

Figure 6. Measurement (blue circles) and simulation (red squares) for $B_{\mathrm{sol}} = 4.5\,\mathrm{T}$. The simulation was normalized so that the rate at $E_{\mathrm{sur}} = E - qU_{\mathrm{PS}} = 0.5\,\mathrm{keV}$ is 1. The experimental rate was normalized so that its average rate is equal to the average of the simulated rate. Only simulation values where a measurement exists were considered for this average. The simulation points are shifted to the right by 0.2 keV to make the points distinguishable. The plot shows that our simulation and our measurements are compatible at the percentage level.

Only events within the region of interest $15\,\mathrm{keV} < E < 21\,\mathrm{keV}$ and from this single detector pixel were counted. Comparisons of our six measurement series at keV surplus energies with our simulations are shown in figures 6 and 7. Except for a single measurement ($B_{\mathrm{sol}} = 4.5\,\mathrm{T}$, $r_{\mathrm{cen}} = 0\,\mathrm{cm}$), the detector rates at positive surplus energies always decrease with growing surplus energy $E - qU_{\mathrm{PS}}$. An explanation of this observation is given in section 7.

6. Simulation tools

Analysis of our experimental data is done by comparison to computer simulations. The main components of our simulations are: (i) electric and magnetic field computations; (ii) electron tracking in vacuum; (iii) electron scattering with H_2 molecules; and (iv) electron tracking in silicon. For the electric field calculations (axisymmetric and three-dimensional, with wires) we used the boundary element method [20]. In order to speed up the simulation in axisymmetric regions, we employed the zonal harmonic expansion method [15]. This turned out to be useful also for the E-GUN–PS geometry, which is not axially symmetric but consists of two

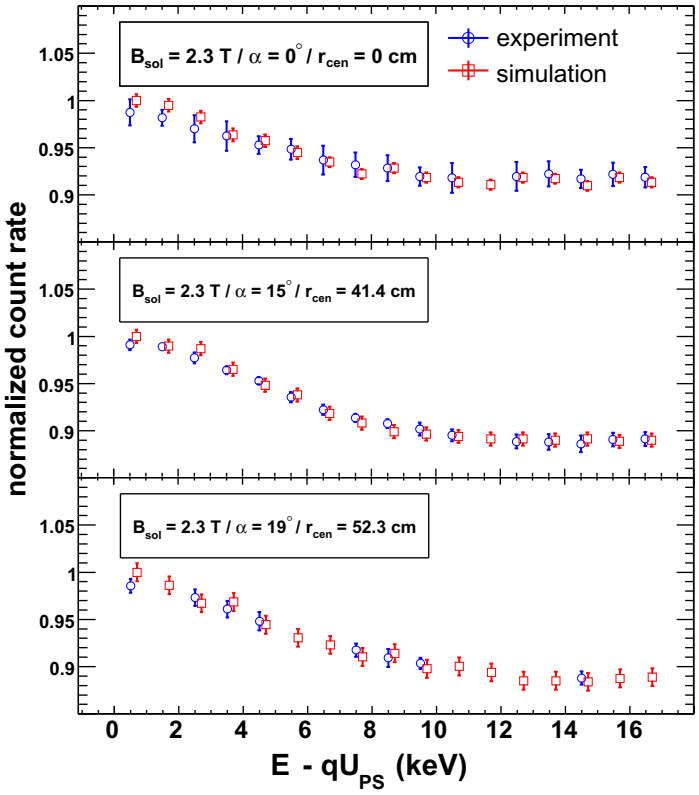

Figure 7. Measurement (blue circles) and simulation (red squares) for $B_{\mathrm{sol}} = 2.3\,\mathrm{T}$. The simulation was normalized so that the rate at $E_{\mathrm{sur}} = E - qU_{\mathrm{PS}} = 0.5\,\mathrm{keV}$ is 1. The experimental rate was normalized so that its average rate is equal to the average of the simulated rate. Only simulation values where a measurement exists were considered for this average. The simulation points are shifted to the right by 0.2 keV to make the points distinguishable. At $\alpha = 19^{\circ}/r_{\mathrm{cen}} = 52.3\,\mathrm{cm}$, we measured at fewer filter potentials. The plot shows that our simulation and our measurements are compatible at the percentage level.

separated, locally axisymmetric regions (E-GUN region and PS region). The zonal harmonic expansion method was also used for magnetic field computations [16]. For electron tracking in vacuum, the exact relativistic equation of motion of the electron with the Lorentz force was employed, using an explicit eighth-order Runge–Kutta method to solve the ordinary differential equations [21]. The electron–H_2 scattering code contains total and differential cross sections [22–30] and MC generation algorithms for elastic, electronic excitation and ionization collisions of electrons with H_2 molecules. Electron detection, electron energies deposited in the sensitive volume of the silicon detector, the detector dead layer and electron backscattering at the detector are modeled by a Monte Carlo C++ code (KESS: KATRIN Electron Scattering in Silicon), which is based on detailed studies [31–34] and agrees well with experimental data.

Our original field calculation, eighth-order Runge–Kutta tracking and e–H_2 scattering C codes [15, 16] have been rewritten into C++ and integrated into the global KATRIN C++ simulation framework 'Kassiopeia' [35]. KESS [36] has also been integrated into Kassiopeia.

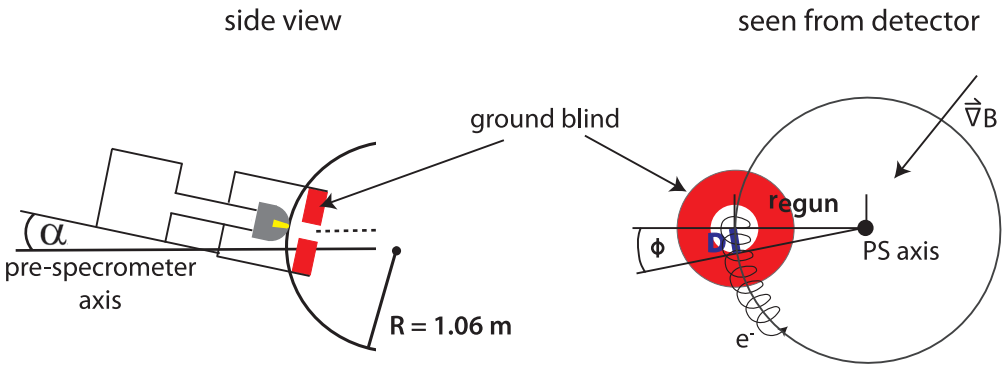

Figure 8. The azimuthal drift in the PS. Left: geometry of the E-GUN. Right: the azimuthal drift seen from the detector side. The electron starts in the center of the bore in the ground blind. Toward the axis of the PS, the B-field is stronger and the curvature of the electron trajectory is larger, resulting in an overall $\vec{B} \times \vec{\nabla} B$ drift around the PS axis (7). If the drift is large enough, the backscattered electron hits the ground blind on its way back from the detector.

We have used both the original C codes and the new Kassiopeia C++ code for the simulations of our paper.

7. Simulation and analysis

Ignoring the influence of the E-GUN and the detector, the PS transmission at keV surplus energies in our codes [15, 16] is always 100%: in order to show this, we injected 130 electrons with uniformly distributed polar and azimuthal angles for $B_{\mathrm{sol}} \in \{2.3\,\mathrm{T}, 4.5\,\mathrm{T}\}$, $U_{\mathrm{electrode}} = U_{\mathrm{tank}} - 0.5\,\mathrm{kV} \in \{-1.5\,\mathrm{kV}, -2.5\,\mathrm{kV}, \ldots, -17.5\,\mathrm{kV}\}$ and $r_{\mathrm{start}} \in \{0\,\mathrm{mm}, 26\,\mathrm{mm}, 37\,\mathrm{mm}\}$ in the entry side magnet ($z = -2.15\,\mathrm{m}$) of the PS. For every simulated electron, the exit condition ($z \geqslant 2.15\,\mathrm{m}$ and $r \leqslant 37\,\mathrm{mm}$) was reached. In the following, we show that the measured decrease of the detector rate at positive surplus energy $E - qU_{\mathrm{PS}}$ is not caused by loss of transmission in the PS, but by the special setup (figure 4) used for the measurements. The transmission probability of 100% can be confirmed only indirectly with an uncertainty at the percentage level via a comparison with a simulation. The ingredients essential for explaining our data are:

(i) a constant PS transmission probability of 100%,
(ii) electron backscattering at the detector,
(iii) $\vec{B} \times \vec{\nabla} B$-drift of electrons proportional to E_{kin} (see (7)),
(iv) reflection of electrons in the electric field of the E-GUN and
(v) The loss of backscattered electrons hitting the ground blind in front of the E-GUN (figures 5 and 8).

Electrons impinging on the detector with an incident energy of $E_{\mathrm{inc}} = 18\,\mathrm{keV}$ and an incident angle of $\theta_{\mathrm{inc}} = 0^{\circ}$ have a probability of about 20% to be backscattered. This probability increases further with larger incident angles [37, 38]. Most of the backscattered electrons have lost their energy in the detector and are again reflected by the filter potential qU_{PS} in the PS or

by the magnetic mirror effect toward the detector. Backscattered electrons having deposited less than $E - qU_{\mathrm{PS}}$ in the detector retain enough energy to pass the filter potential qU_{PS} of the PS in the backward (toward E-GUN) direction. They can enter the E-GUN through the opening in the ground blind (cf figure 5) and can be electrically reflected toward the detector again. This process continues until all the energy is finally deposited inside the detector. Even at high surplus energy $E - qU_{\mathrm{PS}}$, the count rate at the detector remains constant. Flight times in the PS are of the order of 10 ns, which is far below the μs shaping time of the detector electronics. Therefore, only electrons with large energy losses in the dead layer will deposit an energy lower than the region of interest in the sensitive volume. Since all electrons hitting the detector have the same energy and the same angular distribution for all the settings of $U_{\mathrm{electrode}} = U_{\mathrm{tank}} - 0.5\,\mathrm{kV}$, the count rate does not depend on this voltage setting. This explains the measurement at $B_{\mathrm{sol}} = 4.5\,\mathrm{T}$ and $r_{\mathrm{cen}} = 0\,\mathrm{cm}$ ($\alpha = 0^\circ$), where no loss in count rate is observed.

The description above is also valid for the off-axis E-GUN settings with $r_{\mathrm{cen}} \in \{41.4\,\mathrm{cm}, 52.3\,\mathrm{cm}\}$ ($\alpha \in \{15^\circ, 19^\circ\}$).

The axial rotation (7) can cause the electron to eventually hit the ground blind (figure 8), depending on $\vec{B}$, the electron energies $E_\perp$ and $E_\parallel$ and the total path length. The axial rotation is only dependent on energy and has the same sense for a forward (toward detector) and a backward (toward E-GUN) pass of the PS and is therefore adding up at each pass of the PS. The path for the electrons in the PS is elongated by reflections at the detector, at the field of the E-GUN, at magnetic fields and at the spectrometer potential and can thus be multiples of the spectrometer length. The higher the surplus energy, the higher the probability for a backscattered electron to overcome the spectrometer potential after energy deposits in the detector. The higher the surplus energy, the larger the axial rotation that guides electrons onto the ground blind. Therefore, the count rate in the region of interest decreases with higher surplus energy $E_{\mathrm{sur}} = E_0 - qU_{\mathrm{PS}}$. With this, all measurements at $B_{\mathrm{sol}} = 4.5\,\mathrm{T}$ can be explained.

For $B_{\mathrm{sol}} = 2.3\,\mathrm{T}$ a loss in count rate is observed for all E-GUN settings, including the one at $r_{\mathrm{cen}} = 0\,\mathrm{cm}$ ($\alpha = 0^\circ$). It is not possible to explain this effect with backscattering and the $\vec{B} \times \vec{\nabla}|\vec{B}|$ drift alone. The electric field gradient in the E-GUN is large compared to the PS, since a potential difference of 18 kV is applied across a distance of only a few cm. Together with the 50% lower magnetic field in the center of the magnets, this can lead to a non-adiabatic transport in the E-GUN region. At $B_{\mathrm{sol}} = 2.3\,\mathrm{T}$, the E-GUN is located at a magnetic field of $B \approx 0.02\,\mathrm{T}$. Thus, a backscattered electron entering the E-GUN through the ground blind has a probability to change its angle toward the magnetic field line non-adiabatically. Depending on the new angle and the electron energy, it can be trapped between the E-GUN and the closest magnet or the spectrometer potential. Thus, a loss in count rate in the region of interest will also be observed for measurements with r_{cen} ($\alpha = 0^\circ$). This assumption is therefore able to explain the measurement for $B_{\mathrm{sol}} = 2.3\,\mathrm{T}$ and r_{cen} ($\alpha = 0^\circ$).

In our simulations, the electrons were started with a uniform random kinetic energy of $0 < E < 2\,\mathrm{eV}$, and were uniformly distributed on a disc with diameter $d = 1\,\mathrm{mm}$ in front of the actual gold tip. An angular distribution, $\theta = \arcsin(R_1)$ from [39] and $\varphi = 2\pi R_2$ with uniformly distributed random numbers R_1, $R_2 \in [0, 1[$, was used. The time an electron takes to travel between two subsequent detector hits is more than two magnitudes smaller than the DAQ shaping time. This means that subsequent hits are analyzed by the DAQ as one hit. Therefore, each energy deposition in the sensitive detector volume per electron was summed up even for electrons with multiple detector entries. As in the experimental data analysis, all electrons with energy $15 < E < 21\,\mathrm{keV}$ were counted.

Possible exit conditions of the simulation were as follows.

- An electron hits the E-GUN blind (cf figures 5 and 8).
- The electron has energy lower than 100 eV. It is no longer able to pass the dead layer of the detector.
- The electron gets reflected more than 20 times in the PS (trapping).

Figures 6 and 7 show the normalized simulation and experimental results. They show that our simulation can explain the experimental rates at the per cent level. The agreement between experiments and simulations implies that the PS has 100% transmission probability for electrons with keV surplus energy as long as B_{sol} is not smaller than 2.3 T (half the KATRIN design value [5]).

8. Operating the pre-spectrometer at reduced zero filter energy

The previous section proved experimentally that the PS can be operated at reduced or even zero filter energy without essential transmission losses, as long as B_{sol} is not smaller than 2.3 T. In this section, we discuss more generally, with the help of simulations, the operation of PS with zero potential. We will show firstly that, with $U_{\mathrm{PS}} = 0$, the background due to positive ions created by β-electrons is expected to be far below the KATRIN requirement of $b = 10\,\mathrm{mHz}$, and secondly that the electron motion through the PS and MS is fully adiabatic.

Lowering the filter energy qU_{PS} of the PS, the depth of the natural Penning trap, created by the PS and MS retarding potentials U_{PS} and U_{MS} and the magnetic field B_{sol}, between the PS and MS decreases, and the corresponding background level is expected to decrease, too. On the other hand, there is another background component that increases with decreasing qU_{PS}: more β-electrons reach the entrance of the MS. These electrons are not able to produce direct background, but they create positive ions through ionizing collisions with the residual gas molecules. These ions can fly deep into the MS, and can produce low-energy electrons there, either in the residual gas or at the inner surface of the MS electrodes. Some of these electrons can hit the detector, and so we obtain background events. We will present below a quantitative estimate of the maximal value of this background component, in the case of zero PS potential.

Inside the WGTS, 10^{11} electrons are produced through tritium β-decays each second. About 20% of them move through the transport system and reach the entrance of the MS in the case of $qU_{\mathrm{PS}} = 0\,\mathrm{keV}$. Along their way, many of these electrons have ionizing collisions with residual gas molecules and thus produce positive ions. In the absence of any hindrances, all these ions enter the MS. In order to reduce the background rate of these ions, we plan to use an ion-blocking electrode near the center of the MS entrance magnet. Since the positive ions created by ionizing collisions have small kinetic energy (below a few eV), an accordingly small potential barrier created by an ion-blocking electrode would already prevent these ions from entering the MS and thus from producing background.

Nevertheless, the ions created in the region between the ion-blocking electrode and the high-voltage area of the MS are able to enter the MS. We have computed the ion creation rate in this region by detailed trajectory simulations. First, we generated electrons at the center of the MS entrance magnet by using the tritium β-decay Fermi spectrum and an isotropic angular distribution. These electrons were tracked until their reflection at the MS filter potential and then back to their starting point. The ionization probability of an electron was computed by summing

the differential ionization probabilities $d\mathcal{P}_{ion} = \sigma_{ion}(E_{kin}) \cdot n \cdot dl$, where $\sigma_{ion}(E_{kin})$ denotes the ionization cross section of electrons with the residual gas molecules, as a function of the electron kinetic energy E_{kin}; n is the number density of the residual gas and dl the differential pathlength. In our simulations, we assumed molecular hydrogen for the residual gas and we used the e–H_2 ionization cross section formulae of [23, 25] (they are in good agreement with measured e–H_2 cross section values). Assuming $p = 10^{-11}$ mbar pressure and room temperature, the number density is $n = 2.4 \times 10^{11}$ m^{-3}. According to our calculations (simulation of 1000 electron tracks), the average ionization cross section is $\sigma_{ion} = 10^{-21}$ m^2, the average electron path length is $l = 1.5$ m and the average ionization probability of an electron is $\mathcal{P}_{ion} = 3.6 \times 10^{-10}$. Using the 2×10^{10} s^{-1} β-electron intensity, we obtain a positive ion creation rate of roughly $\dot{N}_+ \approx 7$ s^{-1} in the region between the ion-blocking electrode and the high potential domain of the MS.

If an electron is scattered toward large polar angles θ (note that $E_\perp = E_{kin} \cdot \sin^2\theta$), it can become trapped in a hybrid trap near the entrance of the MS: if this electron moves toward the entrance magnet of the MS coming from inside the MS, θ increases adiabatically until $\theta = 90^\circ$ is reached, and the electron starts to move toward the MS again. The MS magnet thus establishes a magnetic mirror for these electrons. Inside the MS, the electron is electrically reflected by the MS filter potential generated by the MS electrode system [40]. In order to compute the ion creation rate due to these trapped electrons, we simulated 10^8 electrons. We used our custom C codes [15, 16] to compute the electromagnetic fields, the trajectories and the e–H_2 scattering. The result of these simulations is the following: the average trapping probability of the β-electrons in the hybrid trap is 3×10^{-11}, and the number of ions created by a trapped electron is smaller than 5 (the trapped electrons can leave the trap by scattering and by energy loss due to synchrotron radiation). From these numbers and from the above β intensity we get an ionization rate that is smaller than 3 s^{-1} . Therefore, the ion creation rate due to these trapped electrons is smaller than that due to the free (non-trapped) electrons.

The ions with a roughly $\dot{N}_+ \approx 10$ s^{-1} rate enter the MS, they will be accelerated to about 18.57 keV kinetic energy, and due to the small (a few Gauss) magnetic field, their motion inside the MS is completely non-adiabatic: they move on a straight line, until they hit the spectrometer tank. During this motion, they can suffer ionizing collisions with the residual gas. The ionizing collision cross section of H^+ and H_2^+ ions of 18 keV kinetic energy with H_2 molecules is about $\sigma_{ion}^+ = 2 \times 10^{-20}$ m^2 [41]. Assuming $l_+ = 20$ m path length for the positive ions inside the MS tank, the secondary electron creation rate due to ionizing collisions of the positive ions with H_2 molecules is $\dot{N}_e = \dot{N}_+ \sigma_{ion}^+ l_+ n = 10^{-6}$ s^{-1}, corresponding to a 0.001 mHz background level. This background increases quadratically with the residual gas pressure, so with $p = 10^{-10}$ mbar the background rate would be 0.1 mHz.

Another background possibility is the following: the ions hit the MS tank with high velocity, and these impact events are connected with secondary electron emission from the surface. One ion can eject more than 1 electron; let us assume that this multiplication number is 10. Then we obtain a secondary electron emission rate of 100 s^{-1} from the tank surface. This is several orders of magnitude smaller than we can expect from cosmic ray muons and environmental radioactivity. Thanks to the magnetic shielding of the approximately axisymmetric magnetic field and to the electric shielding of the wire electrode, only a very small proportion of these electrons is expected to reach the detector; extrapolating the experimental data of the Mainz neutrino mass spectrometer, this proportion could be about 10^{-7}. With this suppression factor, we obtain a 0.01 mHz background level from these electrons.

For both scenarios we obtain a background level caused by positive ions which is several orders of magnitude smaller than the $b = 10\,\mathrm{mHz}$ background value that would be acceptable for the KATRIN experiment [5]. Therefore, our simulations show that the PS could be used with zero potential, without any significant background increase due to the positive ions produced by the β-electrons.

With zero or small PS filter energy, the signal electrons ($E_0 = 18.57\,\mathrm{keV}$) have a high surplus energy $E_{\mathrm{sur}} = E_0 - qU_{\mathrm{PS}}$ inside the PS. Due to the relatively small magnetic field in the middle of the PS ($B_{\mathrm{ana,PS}} = 0.016\,\mathrm{T}$), it could happen, in principle, that the motion of these electrons is not adiabatic. We have checked the adiabaticity behavior of the electrons with detailed trajectory simulations. For this purpose, we started the electrons in the KATRIN source (WGTS) at various points with various polar and azimuthal direction angles, and we tracked them as far as the MS analyzing plane. We defined the starting kinetic energy of the electrons with the following procedure: first, using the starting point, the direction vector and a first estimate for the transmission energy, we computed the guiding center point corresponding to the starting point. Then, we simulated the magnetic field line from the guiding center point until the MS analyzing plane. Using the electric potential and magnetic field values at the two endpoints of this field line, and the starting polar angle, we calculated the adiabatic transmission energy: in the adiabatic approximation, the electron has zero longitudinal energy $E_{\parallel}$ in the analyzing plane (cf figure 2) if it starts with this energy (electrons starting below or above this energy are reflected or transmitted, respectively). We defined the starting kinetic energy of our electrons as the above adiabatic transmission energy plus a small surplus energy ($E_{\mathrm{sur}} = E - qU_{\mathrm{PS}} = 3\,\mathrm{meV}$). If the electron motion is fully adiabatic, $E_{\parallel}$ has to be precisely equal to E_{sur} in the analyzing plane. The main result of our simulations is the following: both for a PS filter energy of $qU_{\mathrm{PS}} = 0\,\mathrm{keV}$ and $qU_{\mathrm{PS}} = 18.3\,\mathrm{keV}$ and for all starting parameters, using the standard KATRIN magnetic field values (3.6 T in WGTS, etc), $|E_{\parallel} - E_{\mathrm{sur}}|$ (computed by exact tracking) is in the MS analyzing plane on the average 0.2 meV, which is four orders of magnitude smaller than the resolution $\Delta E_{\mathrm{MS}} = 0.93\,\mathrm{eV}$ of the KATRIN MS. Therefore, we can say that the motion of signal electrons in the KATRIN system is practically adiabatic, even with $U_{\mathrm{PS}} = 0\,\mathrm{kV}$; deviations from adiabaticity have a negligible effect on the KATRIN transmission function. Note that the electron motion is approximately adiabatic even if the magnetic field in the whole KATRIN system is half of its standard design value; in this case, $|E_{\parallel} - E_{\mathrm{sur}}|$ is in the MS analyzing plane on the average 0.6 meV.

The local behavior of the quantity $\gamma\mu$ was considered to be adiabatic invariant in section 3. There, the difference between the electron energy E and the filter energy qU_{f} was assumed to be small (some tens of eV). As can be seen in figure 9, $\gamma\mu$ has an oscillation behavior due to the superposition of the cyclotron motion and azimuthal magnetron motion; the oscillation period in figure 9 is equal to the electron cyclotron period. The amplitude of the oscillation depends on the electron surplus energy $E_{\mathrm{sur}} = E - qU_{\mathrm{PS}}$: with $E_{\mathrm{sur}} \approx 0.3\,\mathrm{keV}$ in the PS, the relative fluctuation $\delta\gamma\mu/\gamma\mu$ inside the PS is of the order of 10^{-2} (for a smaller starting polar angle θ the fluctuation is somewhat larger), but with E_{sur} of a few keV this fluctuation is much larger, of the order of 1 in figure 9.

How is it then possible that $\gamma\mu$ regains its starting value, despite its large oscillations in the small magnetic field region? The explanation is the following [42–44]: the real adiabatic invariant I_{ad}, which is constant in the adiabatic approximation throughout the whole trajectory, is not $\gamma\mu$, but a complicated function of higher field derivatives. Inside homogeneous field regions the field derivatives are small, and there $I_{\mathrm{ad}} \approx \gamma\mu$. When an electron moves from one

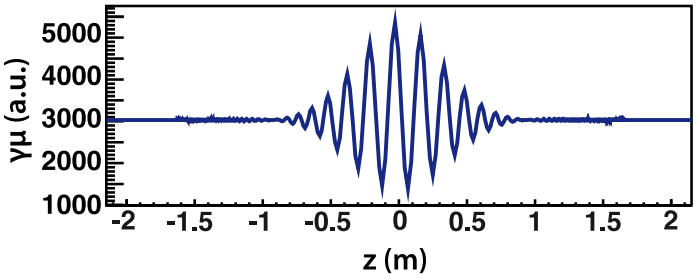

Figure 9. Oscillations of $\gamma\mu$, regaining the original value: $B_{\rm sol} = 4.5\,{\rm T}$, $U_{\rm PS} = -1.5\,{\rm kV}$, $E = 18\,{\rm keV}$, $z_{\rm start} = -2.15\,{\rm m}$, $\varphi_{\rm start} = 60^\circ$ (azimuthal angle), $\theta_{\rm start} = 72^\circ$ (polar angle) and $r_{\rm start} = 26\,{\rm mm}$. The PS solenoids are at $z = -2.15\,{\rm m}$ and $z = +2.15\,{\rm m}$. The radius of the KATRIN flux tube in solenoids is 37 mm at $B_{\rm sol} = 4.5\,{\rm T}$.

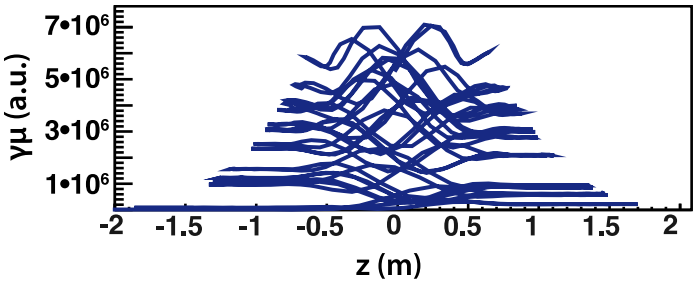

Figure 10. Evolution of $\gamma\mu$ for a trapped electron: $B_{\rm sol} = 0.57\,{\rm T}$, $U_{\rm PS} = -1.5\,{\rm kV}$, $E = 18\,{\rm keV}$, $z_{\rm start} = -2.15\,{\rm m}$, $\varphi_{\rm start} = 30^\circ$ (azimuthal angle), $\theta_{\rm start} = 72^\circ$ (polar angle) and $r_{\rm start} = 26\,{\rm mm}$. The PS solenoids are at $z = -2.15\,{\rm m}$ and $z = +2.15\,{\rm m}$. The radius of the KATRIN flux tube in solenoids is 37 mm at $B_{\rm sol} = 4.5\,{\rm T}$.

homogeneous field region to another, if the adiabatic invariant $I_{\rm ad}$ is constant, $\gamma\mu$ can regain the starting value with high accuracy, although between these two regions, where the field gradients are large, $\gamma\mu$ can have large oscillations. Using a human analogy, we can say that the electron seems to have 'memory', remembering its initial value of $\gamma\mu$ [44]. If the electron motion is not adiabatic (in the case of high energy or small magnetic field), $I_{\rm ad}$ is not constant, so in this case the electron will not gain back its original $\gamma\mu$ value in the second homogenous field region; then, the electron has no memory.

In order to illustrate this phenomenon, we simulated electrons starting from the entry-side magnet of the PS. At the KATRIN field of $B_{\rm sol} = 4.5\,{\rm T}$ (figures 1 and 4), electrons are transmitted through the PS, and $\gamma\mu$ regains its original value (figure 9). If we choose a deliberately low field $B_{\rm sol} = 0.57\,{\rm T}$ in the simulations, electrons can be magnetically trapped and $\gamma\mu$ becomes chaotic (figure 10). If $\gamma\mu$ regains its original value, the angle θ is approximately determined by equation (3). Let us consider an electron that enters the PS in the entry-side magnet with $\theta < 90^\circ$ and for which the polar angle θ is determined by equation (3). In this case, the electron will never acquire $\theta = 90^\circ$ anywhere in the PS. Thus, it cannot be magnetically reflected (figure 11). On the other hand, if equation (3) is violated as shown in figure 10, the

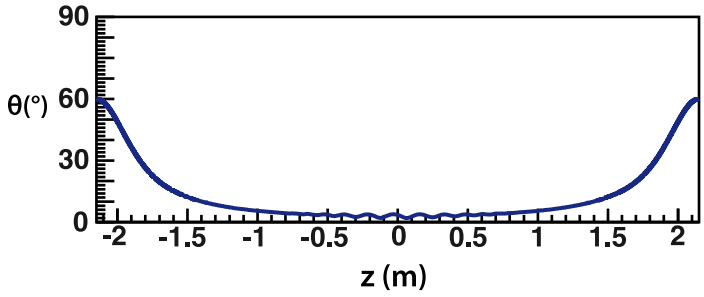

Figure 11. Evolution of the polar angle θ for a transmitted electron. Parameters are as in figure 9.

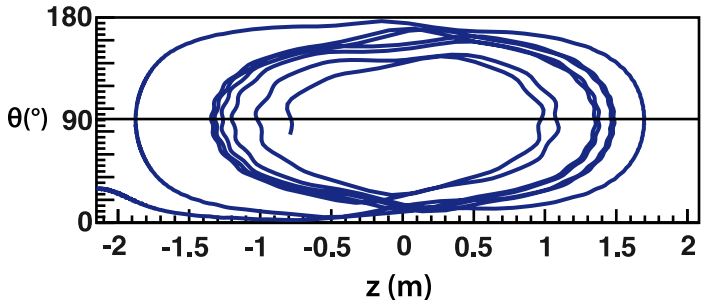

Figure 12. Evolution of the polar angle θ for a trapped electron. Parameters are as in figure 10.

reflection angle $\theta = 90^\circ$ can be reached over and over again (figure 12), and the electron is magnetically trapped inside the PS. It is not transmitted and so it is not detected.

We wish to mention that, at the edge of the outer field lines of the flux tube, with $B_{\mathrm{sol}} = 4.5\,\mathrm{T}$ and zero PS potential, 18 keV electrons inside the PS possess about 2° magnetron motional rotation around the beam axis. This has to be taken into account for precise imaging investigations of the KATRIN experiment (see [8] for experimental examples of a much larger magnetron motional rotation).

The background as a function of the PS potential will be investigated experimentally when the whole KATRIN system is finished. Similarly, the MS transmission function and thus the adiabaticity of the electrons in PS and MS can be experimentally investigated rather precisely, as a function of PS potential, if the PS and MS are connected to each other (by shooting E-GUN electrons through them). The experiments presented in this paper, using only the PS, are sensitive only to large deviations from adiabaticity (small non-adiabaticity effects do not cause any transmission losses in the case of large surplus energies).

9. Conclusion and outlook

Measurement of the absolute neutrino mass scale provides important experimental information to particle physics and cosmology. The KATRIN experiment will investigate this mass scale in a model-independent way with a sensitivity of 200 meV (90% CL). For this purpose it will operate two electrostatic retarding spectrometers. The larger MS and the smaller PS can be elevated to about $-18\,\mathrm{kV}$ high voltage, with a region of zero potential and high magnetic field between

them. In this configuration electrons can be trapped between the spectrometers. Due to many ionizing collisions with residual gas molecules, these trapped electrons increase the background and thus reduce the sensitivity of the experiment. A countermeasure for this background is to operate the PS at a reduced filter energy to decrease the deepness of this trap.

By a combination of test measurements with the PS operated in a separate beamline and detailed MC simulations, we have shown that the PS has excellent transmission properties with reduced filter energy. Our simulations show that the KATRIN experiment can be operated even with zero PS potential; in this case, the signal electrons are transmitted fully adiabatically, and the overall background rate due to the β-electrons is expected to be much smaller than the design value of 10 mHz.

The actual value of the PS filter energy qU_{PS} to minimize KATRIN's background has to be determined experimentally with the full KATRIN setup. It is possible that the final KATRIN setup will operate with a mixture of reduced PS filter energy and other active measures removing the stored electrons from the Penning trap between PS and MS. Sweeping a wire through the trapping volume [9] has proven to be an efficient means of emptying the trap. It will take about $t_{\mathrm{wire}} = 1$ s for the wire to sweep across the magnetic flux tube imaged on the detector. In order to scan the tritium β-spectrum, the MS retarding voltage U_{MS} will be changed every few minutes. The sweeps will be performed during these voltage changes to avoid loss of measurement time. However, the corresponding 10^6 motion cycles is a very large number for a UHV compatible device.

For KATRIN, the transmission function of the PS has to be known with sufficient accuracy [5]. Our investigations indicate that this precision is possible only if the influence of multiple electron reflections at the electron source is suppressed. This can be achieved with (a) a stable, pulsed electron source at the entry of the PS, (b) the PS and MS in their final tandem configuration (cf figure 1) and (c) KATRIN's final detector having a time resolution of about 100 ns.

A novel, angular selective pulsed UV laser photoelectron source, which can produce pulses as short as 40 ns with a repetition rate of up to 10 kHz, is currently being built for KATRIN on the basis of [45–47]. In the experiment we propose, the MS will be operated so that the electrons retain only a few eV surplus energy in the MS and are therefore guaranteed to be transmitted if the MS performs as it should. The filter energy of the PS will be varied, just as in our experiment. In this configuration, multiple (up to about 14) reflections between the detector and the MS potential will cease after less than 20 μs. The fraction of backscattered electrons that retain enough energy to pass the MS filter potential in the backwards (toward the electron source) direction and could possibly get lost at the electron source are negligible in this configuration. Therefore, analysis of this experiment will be much simpler than in our case.

Acknowledgments

The authors thank the Kassiopeia development team at KIT and MIT for their valuable work, for performing the simulations and therefore for the analysis that made this paper possible. The pre-spectrometer team, Stefan Kern, Patrick Krämer, Alan Kumb, Luisa Schäfer and Hans Skacel, could always be counted on and were of great help in keeping the experiment operational. MP thanks Rainer Gumbsheimer for his hospitality at KIT, for numerous discussions, and for his advice and support. We thank Ernst Otten for carefully reading the manuscript and

for valuable comments. This work was supported by the German Ministry for Education and Research (BMBF) under contract numbers 05A08PM1 and 05A08VK2 and by the Deutsche Forschungsgemeinschaft via Transregio 27 'Neutrinos and beyond'.

References

[1] Hannestad S 2012 *Prog. Part. Nucl. Phys.* **65** 185–208
[2] Barabash A 2011 *Phys. Part. Nucl.* **42** 613–27
[3] Gomez-Cadenas J, Martin-Albo J, Mezzetto M, Monrabal F and Sorel M 2012 *Riv. Nuovo Cimento* **35** 29–98
[4] Otten E W and Weinheimer C 2008 *Rep. Prog. Phys.* **71** 086201
[5] Angrik J *et al* 2004 *FZKA Scientific Report* 7090 http://www-ik.fzk.de/katrin
[6] Kraus C *et al* 2005 *Eur. Phys. J.* C **40** 447–68
[7] Aseev V N *et al* 2011 *Phys. Rev.* D **84** 112003
[8] Picard A *et al* 1992 *Nucl. Instrum. Methods* B **63** 345–58
[9] Beck M *et al* 2010 *Eur. Phys. J.* A **44** 499–511
[10] Picard A *et al* 1992 *Z. Phys.* A **342** 71–8
[11] Thümmler T 2010 *PhD Thesis* University of Münster, Germany (http://miami.uni-muenster.de/servlets/DerivateServlet/Derivate4212/diss_thuemmler.pdf)
[12] Lehnert B 1964 *Dynamics of Charged Particles* (Amsterdam: North-Holland)
[13] Jackson J D 1999 *Classical Electrodynamics* (New York: Wiley)
[14] Fränkle F 2010 *PhD Thesis* University of Karlsruhe, Germany (http://digbib.ubka.uni-karlsruhe.de/volltexte/1000019392)
[15] Glück F 2011 *Prog. Electromagn. Res.* B **32** 319–50
[16] Glück F 2011 *Prog. Electromagn. Res.* B **32** 351–88
[17] Anderson P 1959 *Phys. Rev.* **115** 553–4
[18] Wüstling S, Armbrust T, Steidl M and Zadorozhny S 2006 *Nucl. Instrum. Methods* A **568** 382–7
[19] Wall B 2006 *IEEE Nuclear Science Symp. Conf. Record (2006)* vol 1 pp 204–7
[20] Corona T J 2009 Tools for electromagnetic field simulation in the KATRIN experiment *Master's Thesis* MIT
[21] Verner J H *SIAM J. Numer. Anal.* **15** 772–90
[22] Ford A and Browne J 1973 *Chem. Phys. Lett.* **20** 284–90
[23] Hwang W, Kim Y K and Rudd M E 1996 *J. Chem. Phys.* **104** 2956–66
[24] Komasa J and Thakkar A J 1994 *Phys. Rev.* A **49** 965–8
[25] Liu J W 1973 *Phys. Rev.* A **7** 103–9
[26] Liu J 1987 *Phys. Rev.* A **35** 591–7
[27] Liu J 1985 *Phys. Rev.* A **32** 1384–94
[28] Rudd M *et al* 1993 *Phys. Rev.* A **47** 1866–73
[29] Tawara H *et al* 1990 *J. Phys. Chem. Data* **19** 617–36
[30] Trajmar S, Register D F and Chutjian A 1983 *Phys. Rep.* **97** 219–356
[31] Chaoui Z, Ding Z and Goto K 2009 *Phys. Lett.* A **373** 1679–82
[32] Chaoui Z and Azli T 2010 *Surf. Interface Anal.* **42** 1089–92
[33] Chaoui Z and Goto K 2010 *Surf. Interface Anal.* **42** 1105–8
[34] Chaoui Z and Renschler P 2010 *Surf. Interface Anal.* **42** 1093–5
[35] Babutzka M *et al* 2010 *KATRIN Internal Report*
[36] Renschler P 2011 *PhD Thesis* University of Karlsruhe, Germany (http://digbib.ubka.uni-karlsruhe.de/volltexte/1000024959)
[37] Darlington E 1975 *J. Phys. D: Appl. Phys* **8** 85–93
[38] Drescher H, Reiner L and Seidel H 1970 *Z. Angew. Phys.* **29** 331
[39] Pei Z and Berglund C N 2002 *Japan. J. Appl. Phys.* **41** L52–L54
[40] Prall M *et al* 2012 in preparation

[41] Tabata T and Shirai T 2000 *At. Data Nucl. Data Tables* **76** 1–25
[42] Clemmow P and Dougherty J 1969 *Electrodynamics of Particles and Plasmas* (Reading, MA: Addison-Wesley)
[43] Dendy R (ed) 1993 *Plasma Physics: An Introductional Course* (Cambridge: Cambridge University Press)
[44] Northrop T G 1963 *The Adiabatic Motion of Charged Particles* (New York: Interscience)
[45] Valerius K *et al* 2009 *New J. Phys.* **11** 063018
[46] Hugenberg K 2010 *Prog. Part. Nucl. Phys.* **64** 288–90
[47] Valerius K *et al* 2011 *J. Instrum.* **6** P01002